Russian Physics Journal, Vol. 53, No. 8, 2011

CONDENSED-STATE PHYSICS

MICROSTRUCTURE OF Mo – 47% Re – 0.4% Zr ALLOYS AFTER ROLLING AT ROOM TEMPERATURE. II. PECULIARITIES OF MECHANICAL TWINNING AND FORMATION OF HIGH-ANGLE BOUNDARIES BETWEEN MICROBANDS

I. A. Ditenberg,[1,2] A. N. Tyumentsev,[1,2,3] and Ya. V. Shuba[2]

UDC 539.23; 539.216.1; 548.4

It is shown that the Mo – *47%* Re – *0.4%* Zr *alloy after rolling deformation ($\varepsilon \approx 90\%$) at room temperature exhibits certain characteristic features, such as increased density of deformation defects with considerably faceted noncoherent boundaries and reorientation microbands with a specific range of high-angle disorientations around the direction of the ⟨110⟩ type. Using the concepts on direct-plus-reverse (along alternative systems) martensitic transformations as the mechanisms of plastic deformation and crystal-lattice reorientation, an analysis of possible mechanisms for formation of these states is made.*

Keywords: electron microscopy, large plastic deformations, nanostructured states, evaluation of microstructure, plastic deformation mechanism, submicrocrystalline materials, twinning, crystal lattice curvature, disclinations, continual theory of defects.

INTRODUCTION

It was shown in the first part of this study [1] that in the course of rolling of the Mo – 47% Re – 0.4% Zr (wt.%) alloy at room temperature up to the strain value $\varepsilon \approx 90\%$ it exhibited formation of deformation microtwins and nanostructured state with a high density of microbands with high-angle disorientation boundaries parallel to the rolling plane. The features of the internal structure of these microbands (high crystal-lattice curvature and disclination density in the fragments with low-angle disorientation boundaries) allowed us to draw a conclusion that it is the disclination mechanism which underlies crystal-lattice reorientations in the course of formation of these fragments. Below we present the results of investigation of peculiar features of mechanical twinning and formation of high-angle boundaries in the nanostructured state.

RESULTS OF INVESTIGATION

Special features of mechanical twinning

Mechanical twinning is one of the main mechanisms of plastic deformation of rhenium-doped alloys based on the elements of Group VIA of the periodic table of elements. It was shown in [2, 3] that in the Mo–Re and W–Re alloys

[1]Institute of Strength Physics and Materials Science of the Siberian Branch of the Russian Academy of Sciences, Tomsk, Russia, [2]Tomsk State University, Tomsk, Russia, [3]V. D. Kuznetsov Siberian Physical-Technical Institute of Tomsk State University, Tomsk, Russia, e-mail: tyuments@phys.tsu.ru. Translated from Izvestiya Vysshikh Uchebnykh Zavedenii, Fizika, No. 7, pp. 46–53, July, 2010. Original article submitted June 30, 2009; revision submitted January 22, 2010.

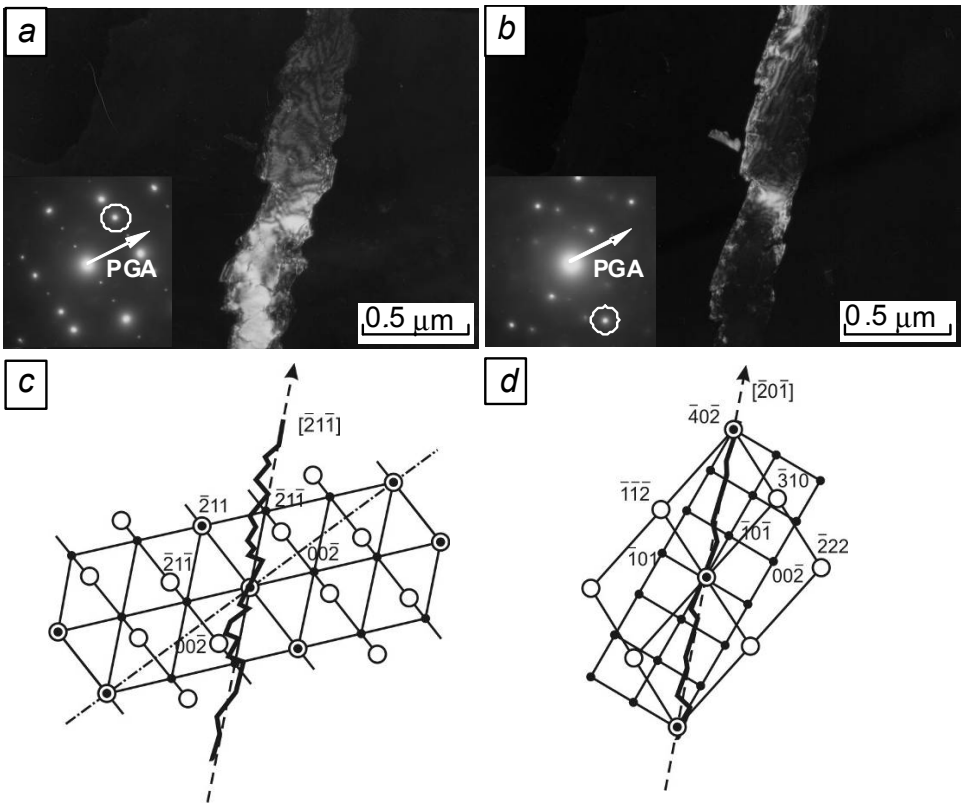

Fig. 1. Dark-field images (in circled reflections) from a $\{\bar{2}11\}$ deformation twin and the respective microdiffraction patterns (*a*, *b*) and electron-diffraction patterns (*c*, *d*) for different foil orientations in the microscope. Matrix reflexes (open circles), twin reflexes (filled circles), goniometer tilt angle – 0°, matrix and twin zone axes – [120] (*a*, *c*), and goniometer tilt angle – 34°, matrix zone axis – ≈[010], twin zone axis ≈$[13\bar{2}]$ (*b*, *d*). Dash-dot-line – projection of the trace of a coherent twin boundary in the $\{\bar{2}11\}$ plane.

mechanical twinning is the principal mechanism in the initial stage of plastic deformation at low temperatures, which affects the temperature dependence of the yield strength within the low-temperature range. According to the data in [4], mechanical twinning, on the one hand, results from the reduced stacking-fault energy during rhenium doping of chromium, molybdenum and tungsten; on the other hand, it is a major cause for the so-called rhenium effect – a sharp increase in plasticity as a result of this doping.

Deformation twins, revealed in this study, can propagate along a variety of twinning systems. They are tenths fractions of micron wide and a few microns long. It should be noted that apart from deformation twins with coherent boundaries in the habitus plane {112} typical for bcc-materials, there is a large number of microbands with a reorientation vector of the twinning type ($\boldsymbol{\theta}$ = 180°<112>), which have noncoherent boundaries (lying outside the twinning planes). Since these boundaries do not represent planes of specula crystal-lattice reflections, strictly speaking, they are not twins. Nonetheless, based on the twinning nature of reorientation, they will be referred to here as deformation microtwins.

An example of a microtwin is given in Fig. 1. It is evident that a characteristic feature of this microtwin is a complex faceted structure of its boundaries. Note that the trace from the plane of a coherent twin boundary would not coincide with either the twin as a whole (dotted line in Fig.1*c*) or the prevailing number of face boundaries. It follows from the analysis presented in Fig. 1 that the habitus plane of the microtwin in question is $[\bar{1}02]$ (crossproduct of the vectors, $[\bar{2}1\bar{1}]$ and $[\bar{2}0\bar{1}]$, lying in this plane), which forms an angle of ≈ 43° with the plane of the coherent twin boundary.

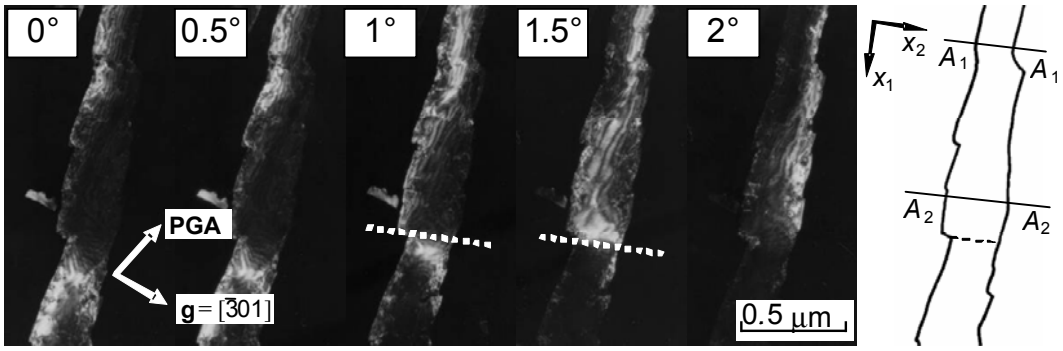

Fig. 2. Extinction contour displacement within the deformation microtwin during tilting of the specimen in the goniometer.

An important feature of the internal structure of microtwins with noncoherent (off-plane) boundaries is the presence of highly defective structure states with high crystal-lattice curvature and curl. Shown in Fig. 2 is an example of a dark-field analysis of the curvature inside the above-described microtwin, performed for the [$\bar{3}$01] reflection circled in Fig. 1*b*.

It is evident from the figure that when the specimen is tilted in the goniomer by the angle $\Delta\varphi \approx 2°$ the extinction contour in the twin cross-section (A_1A_1) is displaced by $\Delta r \approx 0.14$ μm, and for the goniometer tilt angle $\Delta\varphi \approx 1°$ it is displaced by 0.22 μm in the cross-section (A_2A_2). Note that the angle between the current reflection $\boldsymbol{g}$ = [$\bar{3}$01] and the projection of the goniometer tilt axis (**PGA**, see Fig. 2) $\beta \approx 85°$. Now, in accordance with formula (1) in the first part of this study [1] the curvature tensor component χ_{21} (characterizing the crystal-lattice curvature of a plane parallel to the foil plane, see Fig. 1 in [1]) in the (A_1A_1) cross-section will be $\chi_{21} \approx 14$ deg/μm, while decreasing down to $\chi_{21} \approx 4.5$ deg/μm close to the (A_2A_2) deformation microtwin cross-section. Note that the extinction contour widths (L) in the cross-sections (A_1A_1) and (A_2A_2) are about 0.13 and 0.19 μm, respectively. Then, according to Eq. (2) from Part I of this study, for the foil thickness $\Delta t \approx 0.15$ μm and $\Delta\gamma \approx 0.5°$ the curvature component χ_{31} (see Fig. 1 in [1]) would decrease within $\Delta x_1 \approx 0.7$ μm between the above cross-sections from ≈8.3 to 2.3 deg/μm.

Thus, apart from the high crystal-lattice curvature, there are considerable curvature gradients inside the microtwin. Being averaged within the above interval, they reach the values as high as $\partial\chi_{21}/\partial x_1 \approx 13.6$ deg/μm^2 and $\partial\chi_{31}/\partial x_1 \approx 8.6$ deg/μm^2 and are summands of the curvature curl components: $-(\partial\chi_{21}/\partial x_1 - \partial\chi_{11}/\partial x_2)$ and $-(\partial\chi_{31}/\partial x_1 - \partial\chi_{11}/\partial x_3)$. Since the extinction contour under study is nearly parallel to the x_1 axis and its diffraction contrast intensity along this axis is practically unchanged, the curvature component χ_{11} in the zone of this contour would approximate zero. Then $|\chi_{11}| << |\chi_{21}|$ and $|\chi_{31}|$, $|\partial\chi_{11}/\partial x_2| << |\partial\chi_{21}/\partial x_1|$ and $|\partial\chi_{11}/\partial x_3| << |\partial\chi_{31}/\partial x_1|$. Therefore,

$$-(\partial\chi_{21}/\partial x_1 - \partial\chi_{11}/\partial x_2) \approx 13.6 \text{ deg./}\mu\text{m}^2, \quad (1)$$

$$-(\partial\chi_{31}/\partial x_1 - \partial\chi_{11}/\partial x_3) \approx 8.6 \text{ deg./}\mu\text{m}^2. \quad (2)$$

These experimentally obtained quantities include elastic and plastic components of crystal-lattice distortion. It should be noted that the plastic components, according to the continual defect theory [5–7], are the components of the continual disclination density tensor

$$\Omega_{31} = -(\partial\chi_{21}^{Pl}/\partial x_1 - \partial\chi_{11}^{Pl}/\partial x_2), \quad (3)$$

$$\Omega_{21} = -(\partial\chi_{31}^{Pl}/\partial x_1 - \partial\chi_{11}^{Pl}/\partial x_3). \quad (4)$$

Earlier, similar structure states were observed in submicrocrystalline titanium nitride [8] and copper [7, 9]. In [10, 11], it was proposed to characterize this state as a structure state with high continual disclination density.

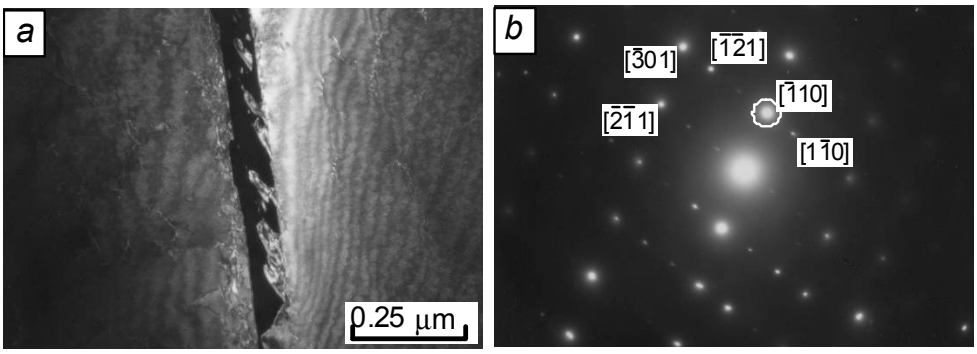

Fig. 3. Dark-field images (in the matrix reflection $[\bar{1}10]$) of a deformation microtwin containing microvolumes of untwinned crystal, $\varepsilon \approx 90\%$. The cross-section is parallel to the plane of rolling; $[\bar{1}10]$ and $[\bar{3}01]$ – reflections from the matrix, [113]; $[1\bar{1}0]$ and $[\bar{1}\bar{2}1]$ – reflections from the microtwin, zone axis $[\bar{1}\bar{1}3]$, and total reflection – $[\bar{2}\bar{1}1]$.

Schematically, the disclination model of formation of this state is given in [1] in Fig. 4*a* and *b*. It is evident from the figure that, for one thing, this state is the first stage of formation of a boundary with a variable disorientation vector, and, secondly, it gives rise to local internal stresses and stress gradients similar to those observed in the vicinity of this boundary. Their values can be estimated by the formulas similar to Eq. (4) and (5) used in [1], substituting the tensor curvature gradient for the vector reorientation gradient. Then, for estimation of the local stress field inside the microtwin uder study the following formulas could be used:

$$\partial\sigma_{loc}/\partial x_1 \approx (E/2\pi)\times(\partial\chi_{21}/\partial x_1), \tag{5}$$

$$\sigma_{loc} \approx (E\times\Delta x_1/2\pi)\times(\partial\chi_{21}/\partial x_1). \tag{6}$$

Substituting the above experimental values of $\partial\chi_{21}/\partial x_1$ and Δx_1 into these expressions, we obtain the local stress field characteristics close to those obtained inside the reorientation bands in [1]

$$\partial\sigma_{loc}/\partial r \approx E/30\ \mu m^{-1},$$

$$\sigma_{loc} \approx E/50.$$

Moreover, the dark-field analysis of reorientations showed that in addition to the above-mentioned substructure with high continuous reorientations, discrete reorientation boundaries are observed in microtwins, which devide them lengthwise into fragments with low-angle boundaries. One of these boundaries is illustrated in Fig. 2 by dashed lines.

The electron microsopy investigations also revealed a large number of microtwins containing islands of untwinned material clearly seen in Fig. 3*a* in the dark-field image of the matrix reflection.

High-angle boundaries of microband structure

A specific feature of high-angle boundaries of microbanded structure consists in a large fraction of boundaries with reorientation vectors around the direction of the ⟨110⟩ type. An example of this boundary with the reorientation vector $\boldsymbol{\theta} \approx 35°[\bar{1}\bar{1}0]$ is presented in Fig. 2 in [1]. In Fig. 4, we show a high-angle boundary of a microband with the reorientation vector $\boldsymbol{\theta} = (50–60)°[\bar{1}10]$, which was observed in the cross-section parallel to the plane of rolling. The boundary is parallel to this plane; hence it is not seen in the electron microimage and is revealed by the presence of two zone axes in the electron diffraction pattern. As follows from the analysis of the latter (Fig. 4*b*), these are the [111] and

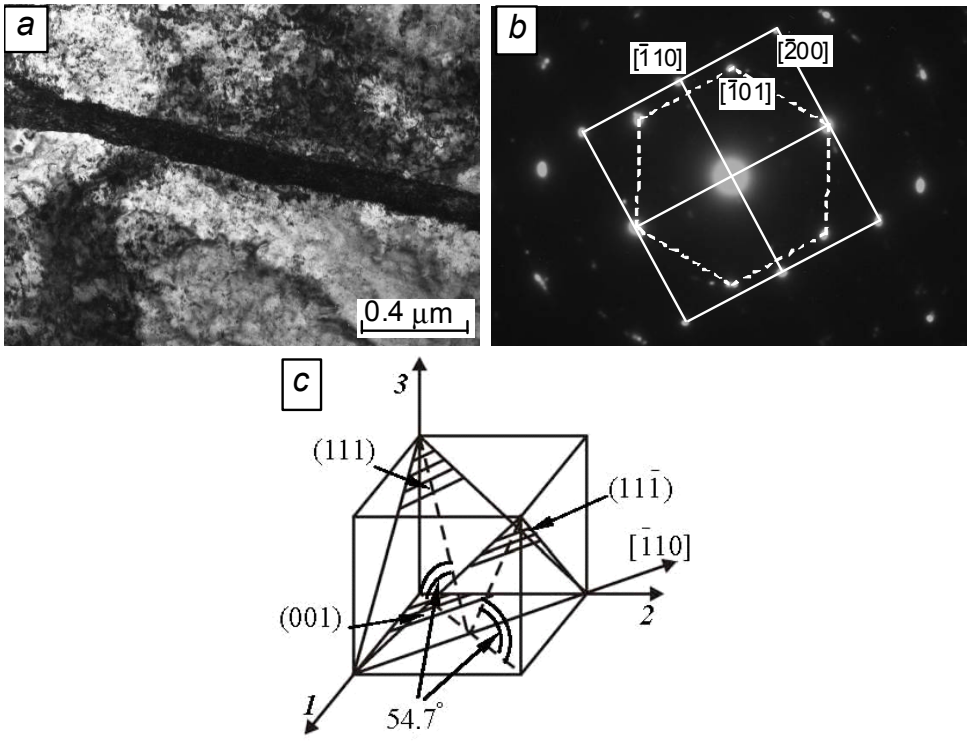

Fig. 4. Bright-field electron-microscopy image (*a*), microdiffraction pattern (*b*) and crystal-lattice reorientation schematics (*c*) in the region of a high-angle boundary with the reorientation vector $\boldsymbol{\theta}$ = (50–60)°[$\bar{1}$10]. The cross section is parallel to the rolling plane. Reflections from the [001] (solid line) and [111] (dotted line) zone axes.

[001] axes with a common current reflection $\boldsymbol{g}$ = [$\bar{1}$10], which corresponds to reorientation of the adjacent regions along [$\bar{1}$10] by an angle close to that between the (111) and (001) planes, which is equal to 54.7° (Fig. 4*c*).

It was shown in [6, 12, 13] that in structural states with high crystal-lattice curvature the accuracy, to which one can determine the local crystal orientation and hence reorientation vectors ($\Delta\boldsymbol{\theta}$), is controlled by the value of $\chi_{ij}\cdot\Delta t$. Here χ_{ij} is the curvature-tensor component characterizing the curvature of crystallographic planes responsible for the extinction-contour contrast and Δt is the foil thickness. In the present work for the values of $\chi_{ij} \le 20$ deg/μm and $\Delta t \le 0.25$ μm, this accuracy is limited by $\Delta\boldsymbol{\theta} \le \pm 5°$. Thus, the values of reorientation vectors at the microband boundaries presented in the above examples lie within $\boldsymbol{\theta}$ = (30–40)°[$\bar{1}$10] and $\boldsymbol{\theta}$ = ±(50–60)°[$\bar{1}$10].

DISCUSSION OF RESULTS

Formation of microband structure of the type described above was observed earlier [12] in a vanadium alloy after rolling at room temperature. An assumption is made in that work that the specific range of disorientations at the microband boundaries is due to their participation in the formation of one of the mechanisms of direct-plus-reverse martensitic-type transformations, with the reverse transformations following alternative systems – the systems with different orientation relationships between the lattices of the initial and martensitic phases. Peculiarities and atomic models of these mechanisms are detailed in a number of reviews [7, 14, and15]. Therefore, here we shall report but only briefly their potential to describe certain phenomena of plastic deformation and crystal-lattice reorientation, and present one of the atomic models of formation of reorientation bands (50–60)°<110> observed in an bcc-crystal in the present work.

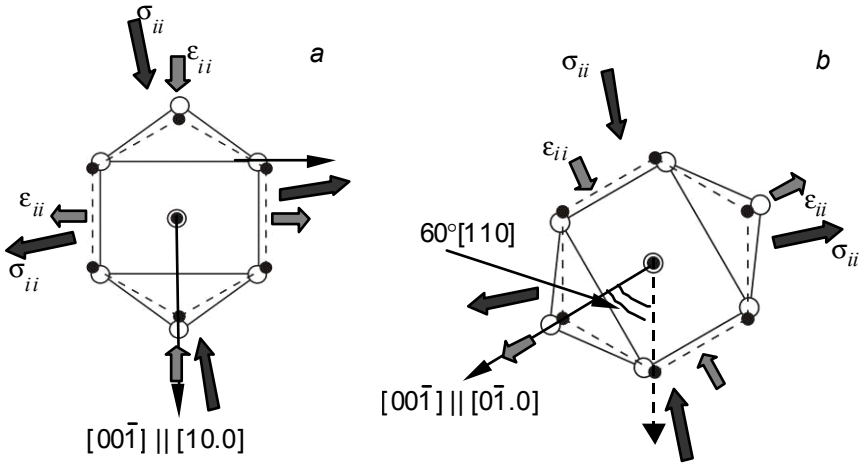

Fig. 5. Schematics of atomic rearrangements in the course of bcc→hcp→bcc-transformation resulting in a 60°[110] reorientation of the crystal lattice. A version of the N–W relation. Atoms of the bcc-phase (light circles) and atoms of the intermediate (martensitic) hcp-phase (dark circles).

To develop the models, the authors of [7, 13–17] used the geometrical theory of martensitic (bcc →fcc and bcc→hcp) transformations (MT) [18], where atomic rearrangements represent combined cooperative atomic shears (shufflings) in close-packed planes of the bcc-lattice and homogeneous deformation of the Bein-type transformation.

Using this model and a variety of versions of the system of reverse transformations varying in the course of bcc→hcp→bcc and fcc→bcc→fcc-transformations, we managed to describe many of the hitherto inexplicit features of plastic deformation. Here belong initiation of partial and complete dislocations in fcc-nanocrystals [19, 20], non-polar mechanisms of mechanical twinning in these materials [19, 20], deformation twinning in the planes with different indices in TiNi alloys [14, 15], formation of localized strain bands with crystal lattice reorientations at ≈ 35°<110> and 60°<110> in austenite steels [13, 14, 16] and, finally, the reorientation bands (50–60)°<110> in bcc-alloys discussed in [12].

An example of formation of these bands in the course of bcc→hcp→bcc-transformations is shown in Fig. 5. In this version, a direct (bcc→fcc, Fig. 5*a*) transformation, apart from cooperative displacements of atomic planes (110) along [$\bar{1}$10] and [1$\bar{1}$0] not shown here (for details, see, e.g., [13, 15–18]), involves homogenous deformation transforming these planes into close-packed hcp-phases, in the case where the Nishiyama-Wassermann (N-W) relation is fulfilled.

In materials with comparatively high phase stability, the intermediate hcp-phase exists only in the course of deformation in the field of high local stresses. Since its formation is a way of relaxation for these stresses, their decrease results in a reverse MT similarly to the case of superplasticity of alloys with thermoelastic MTs. However, unlike reversible deformation under conditions of superplasticity taking place in the course of unloading under the action of residual stresses opposite in the sign to the straining stress, under persistent plastic deformation a reverse MT is developed in the stress field (σ_{ii} in Fig. 5), which in the case of an unchanged system of transformation is its effective obstacle. On the other hand, the presence of an alternative system of reverse transformations ensures a very high probability of a system for which a local stress field would stimulate both direct and reverse transformation. It is evident from Fig. 5 that this version will be the case if the reverse (hcp→bcc, Fig. 5*b*) transformation is accompanied by a change in the direction of deformation of the reverse transformation in the hcp-cell of the martensite phase. Note that the reverse MP is developed not only due to the thermodynamic energy advantage, but also under the action of the local stress (straining) field in the region of transformation, which represents a plastic deformation mode and an additional path for relaxation of these stresses.

Figure 5 presents an example of a bcc→hcp→bcc-transformation resulting in a 60°[110] crystal-lattice reorientation. It was shown in [12, 15, 17] that in the case where the Kurdyumov–Zaks relation is fulfilled in the course

of an MT, the number of alternative systems of reverse transformation is increased, which gives rise to the following versions of reorientations: 10.5°<110>, 49.5°<110>, 60°<110> and 70.5°<110>. Furthermore, multiple direct-plus-reverse transformations are very likely to occur and be followed by multiple crystal-lattice reorientations. This could give rise to an additional increase in the variety of these reorientations. If such a reorientation occurs within the same plane of cooperative atomic displacements, a wider range of disorientations around the ⟨110⟩-type axes observed in the present work can form (see also Ref. [12]).

Note that one of the above versions of the (70.5°<110>) reorientation is from the crystaloographic viewpoint equivalent to the 180°<112> reorientation. Then, a bcc→hcp→bcc-transformation can serve a mechanism of formation of {112} deformation twins. It was shown in [14, 15] that unlike a well-known mechanism of polar mechanical twinning [21], in the case of these twins the coherent twin boundary in the respective plane of the {112} type is not the plane of zero distortions. Therefore, implementation of this mechanism could be viewed as a potential reason for formation of twins (see Figs. 1 and 2) with incoherent boundaries.

If this is the case, then the islands of parent orientation (Fig. 3) observed inside the twins could be microvolumes within which a reverse MT occurs without changing the system of reverse transformation and parent phase orientation. This is the reversible transformation deformation that would give rise to well-known peculiarities of mechanical behavior of Mo–Re and W–Re alloys - a phenomenon of elastic twinning and superplasticity observed in [2–4] at the level of microdeformation of these alloys. It is worth mentioning that the above phenomena can be described on the bases of currently available concepts [14, 15] on inelastic deformation of materials by the mechanisms of reversible martensitic-type transformations rather than reversible motion of partial dislocations.

The physical cause, underlying the above mechanisms of direct-plus-reverse MTs, consists in the phenomenon of phase instability of the crystal in the fields of high ($\sigma_{loc} \approx \approx E/50$) local stresses. These stresses result from high-intensity strain hardening and low efficiency of their relaxation via dislocation mechanisms of deformation in the substructures with high density of defects.

Another possible reason for formation of deformation twins with faceted boundaries lying off the twinning plane are the processes of their interaction with dislocations in the course of plastic deformation following the formation of a twin. According to [21], the mechanisms of such interaction in a bcc-crystal consists in the fact that in the case where glide dislocations of the 1/2 [111]-type cross the twin boundaries, this may result in the formation of steps corresponding to a variety of partial dislocations and complete dislocations inside the twin. Partial dislocations can glide along the twin interface, resulting in the growth of the twin, and form steps changing the habitus plane.

Complete dislocations, depending on the features of the local stress field, can move in the plane of mirror reflection and further beyond the twin boundary in the course of their interactions with the opposite boundary, similarly to the process described above. Second, they can build up inside the twin, in particular, resulting in the formation of substructures with high values of defect density and local internal stresses.

The dislocation model of twinning can also explain the presence of islands of parent orientation inside the twin. According to [21], they could appear via emission of complete dislocations from a noncoherent top of the protruding twin front in order to compensate for the long-range stress field of this front. By interacting with the partial twinning dislocation, the emitted dislocation leaves behind the islands of the parent orientation inside the twin, which are limited by a set of dipoles (for detail see [21]), thus ensuring shear deformation equivalent to that caused by the twin boundary.

Note that these islands, irrespective of the mechanism (dislocation or martensitic) of their formation, constitute of the factors for formation of faceted structure of twin boundaries.

Unfortunately, the results presented in this study do not allow us to give preference to either of the mechanisms (martensitic or dislocation) of formation of twins with noncoherent boundaries. In particular, this is due to considerable experimental difficulties in observing the intermediate martensitic phase, which in the case of direct-plus-reverse MTs would exist only in the fields of local stresses in the course of deformation.

Nevertheless, this mechanism is still an attractive option as a mechanism of deformation and crystal-lattice reorientation, since there has been no alternative explanation of the preferred orientation of microbands about the <110>-type direction with a large fraction of boundaries with the (50–60)°<110> reorientation vectors proposed so far. In the alloy discussed in the present study, there is an additional stimulus for activation of this particular mechanism/ which consists in the fact [1] that its composition lies close to the concentration interval of phase instability – formation of the σ-phase. The structure of this phase can be presented by an hcp-lattice, wherein certain atoms (for the sake of

better packing) are shifted from its basis planes towards intermediate (between the layers) positions. It is also known [4] that a characteristic feature of fine structure of Mo–Re alloys is the formation of atomic systems similar to the σ-phase, which are observed at considerably lower rhenium concentrations (about 30 wt%) compared to that in the Mo – 47% Re – 0.4% Zr alloy.

Also, an application of the mechanism of direct-plus-reverse MTs turns out to be useful in analyzing the so-called rhenium effect – increased plasticity of bcc-alloys of Group VIA of the periodic table, which results from their doing with rhenium, in particular, when discussing the origin of super-high technological plasticity of these alloys at room temperature allowing practically unlimited degree of straining and very high strain-hardening results to be achieved (tensile strength up to 5–7 GPa).

In discussing this phenomenon it is worth mentioning that, as shown in [12–17], the main deformation mode of direct-plus-reverse MTs in the course of formation of reorientation bands and deformation twins in bcc-crystals is homogenous transformation deformation of the Bein-type. Note that the defects of sub-structure hardening (dislocations, low- and high-angle fragment and microband boundaries) while suppressing the dislocation activity, do not serve in the least measure effective obstacles either for the carriers of this deformation mode or crystal-lattice reorientation; and the high local internal stresses representative of large plastic deformations stimulate local martensitic transformations rather than hinder them.

Furthermore, it is well known [22, 23] that under conditions of phase instability (e.g., in the vicinity of martensitic transformation points) one often observes decreased values of elastic moduli. This might result in effective material softening and activation of nearly all so far known deformation modes: dislocation glide as a result of decreased shear stress, diffusion mechanisms of deformation due to lower activation energy of point-defect formation and migration, and collective rotation modes of deformation, which develop using the above mechanisms. Note that processes of relaxation could intensively develop in the zones of non-equilibrium MTs, involving not only fields of local internal stress but also highly defective deformation substructures formed in the course of rolling.

Thus, a most important feature of plastic deformation via the mechanisms of direct-plus-reverse MTs is the absence of any effective obstacles for the carriers of this mode, including the case for super-high degrees of deformation, and a concurrent possibility of intensive relaxation of highly defective structural states formed under these conditions. From our viewpoint, it is the combined action of these factors which results in the rhenium effect – very large (practically unlimited) values of plastic deformation achieved at room temperature.

SUMMARY

1. It has been shown that in the course of nanostructuring of the microstructure of a Mo – 47% Re – 0.4% Zr alloy under conditions of large plastic deformations by rolling at room temperature, principal mechanisms of formation of high-angle disorientation boundaries are those of twinning and formation of microbands with high-angle reorientation boundaries.

2. The characteristic features of the nanostructured state thus formed are found to be, first, preferred character of microband reorientation around the ⟨110⟩ direction with a high density of boundaries with the reorientation vectors, $\theta \approx$ (30–40)°⟨110⟩ and (50–60)°⟨110⟩, and, second, a high density of deformation twins with severely faceted noncoherent boundaries and high values of defect density and local internal stresses.

3. Two versions have been proposed to describe these peculiarities: 1) formation of reorientation microbands and deformation twins via the mechanisms of direct-plus-reverse MTs (following alternative systems) and 2) variations in the twin structure under different conditions of their interaction with glide dislocations and dislocations emitted by the moving noncoherent twin boundary.

This work has been partially funded by The Russian Science Support Foundation, a RBRF grant No. 09-02-00809a, and a RF President grant MK-658.2009.8. The investigations were performed using the facilities of the Tomsk Sharing Center for Materials Science Research of Tomsk State University.

REFERENCES

1. I. A. Ditenberg, A. N. Tyumentsev, and Ya. V. Shuba, Russ. Phys. J., No. 7, 706–715 (2010).
2. O. D. Sheremetiev, Yu. I. Pochivalov, N. I. Freze, and A. D. Korotaev, Doklady Akad. Naur USSR, **203**, No. 3, 643–646 (1972).
3. O. D. Sheremetiev, Yu. I. Pochivalov, A. D. Korotaev, and V. M. Amosov, Metallofizika, No. 44, 16–21, Kiev, Naukova Dumka (1972).
4. V. I. Trefilov, Yu. V. Mil'man, and S. A Firsov, Physical Strength Peculiarities of Refractive Metals [in Russian], Kiev, Naukova Dumka (1983).
5. R. De Witt, The Continual Theory of Disclinations [Russian translation], Moscow, Mir (1977).
6. A. N. Tyumentsev, I. A. Ditenberg, Yu. P. Pinzhin, *et al.,* Fiz. Met. Metalloved., **96**, No. 4, 33–43 (2003).
7. A. N. Tyumentsev, A. D. Korotaev, and Yu. P. Pinzhin, Physical Mesomechanics [in Russian], **7**, No. 4, 35–54 (2004).
8. A. N. Tyumentsev, A. D. Korotaev, Yu. P. Pinzhin, and A. F. Safarov, Russ. Phys. J., No. 7, 613–619 (1998).
9. A. N. Tyumentsev, A. D. Korotaev, I. A. Ditenberg, and Yu. P. Pinzhin, Fundamental Problems of Modern materials Science [in Russian], **2**, No. 4, 69–79 (2005).
10. A. D. Korotaev, A. N. Tyumentsev, and Yu. P. Pinzhin, Physical Mesomechanics [in Russian], **1**, No. 1, 23–35 (1998).
11. A. D. Korotaev, A. N. Tyumentsev, Yu. P. Pinzhin, *et al*., Theor. Appl. Fract. Mech., **35**, 163–169 (2001).
12. A. N. Tyumentsev, Yu. P. Pinzhin, S. V. Ovchinnikov, *et al*., Promising Materials [in Russian], No. 5, 15–36 (2005).
13. A. N. Tyumentsev, I. Yu. Litovchenko, and Yu. P. Pinzhin, Physical Mesomechanics [in Russian], **6**, No. 2, 15–36 (2003).
14. A. N. Tyumentsev, A. D. Korotaev, Yu. P. Pinzhin, *et al*., Russ. Phys. J., No. 8, 818–839 (2004).
15. A. N. Tyumentsev, N. S. Surikova, I. Yu. Litovchenko, *et al*., Acta Mater., **52**, 2067–2074 (2004).
16. A. N. Tyumentsev, I. Yu. Litovchenko, Yu. P. Pinzhin, *et al*., Fiz. Met. Metalloved., **95**, No. 2, 86–95 (2003).
17. A. N. Tyumentsev, N. S. Surikova, I. Yu. Litovchenko, *et al*., *Ibid*., **95**, No. 1, 97–106 (2003).
18. F. A. Kassan-Ogly, V. E. Naish, and I. V. Sagaradze, *Ibid*., **65**, No. 3, 481–492 (1998).
19. A. N. Tyumentsev, I. Yu. Litovchenko, Yu. P. Pinzhin, and N. V. Shevchenko, Doklady Akad. Nauk, **403**, No. 5, 623–626 (2005).
20. I. Yu. Litovchenko, N. V. Shevchenko, A. N. Tyumentsev, and Yu. P. Pinzhin, Physical Mesomechanics [in Russian], **8**, No. 4, 5–12 (2005).
21. J. P. Hirt and J. Lothe, Theory of Dislocations, McGraw-Hill, N.Y. (1968).
22. V. N. Khachin, S. A. Muslov, V. G. Pushin, *et al*., Doklady Akad. Nauk. USSR, **295**, No. 3, 606–609 (1987).
23. K. Enami, J. Nasunuma, A. Nagasawa, and S. Nenno, Scripta Met., **10**, No. 10, 879–884 (1976).